J|A|C|S ARTICLES

Published on Web 11/24/2010

Simultaneous Tailoring of Phase Evolution and Dopant Distribution in the Glassy Phase for Controllable Luminescence

Shifeng Zhou,*,† Nan Jiang,‡ Kiyotaka Miura,*,† Setsuhisa Tanabe,§ Masahiro Shimizu,† Masaaki Sakakura,† Yasuhiko Shimotsuma,† Masayuki Nishi,† Jianrong Qiu,|| and Kazuyuki Hirao†

Department of Material Chemistry, Graduate School of Engineering, Kyoto University, Nishikyo-ku, Kyoto 615-8510, Japan, Department of Physics, Arizona State University, Tempe, Arizona 85287-1504, United States, Graduate School of Human and Environmental Studies, Kyoto University, Yoshida-Nihonmatsu-Cho Sakyo-ku, Kyoto 606-8501, Japan, and Department of Materials Science and Engineering, Zhejiang University, Hangzhou 310027, China

Received September 25, 2010; E-mail: zhoushifeng@curl1.kuic.kyoto-u.ac.jp; kmiura@collon1.kuic.kyoto-u.ac.jp

Abstract: Construction of an active composite with multicolor visible and broadband near-infrared luminescence is of great technological importance for various applications, including three-dimensional (3D) display, broadband telecommunication, and tunable lasers. The major challenge is the effective management of energy transfer between different dopants in composite. Here we present an *in situ* strategy for controlling energy transfer between multiple active centers via simultaneous tailoring of the evolution of phases and the distribution of dopants in the glassy phase. We show that the orderly precipitation of Ga_2O_3 and LaF_3 nanocrystals and the selective incorporation of Ni^{2+} and Er^{3+} into them can be achieved. The obtained composite shows unique multicolor visible and broadband near-infrared emission. Possible mechanisms for the selective doping phenomenon are proposed, based on thorough structural and optical characterizations and crystal-field calculation results. Moreover, the strategy can be successfully extended to accomplish space-selective control of multicolor luminescence by employing the modulated stimulation field. The results suggest that the strategy could be applied to fabricate a multifunctional light source with a broad range of important host/activator combinations and to construct various types of three-dimensional active microstructures.

Introduction

The ability to manipulate the electron transition process of active dopants in nanomaterials is fundamental to photonic applications. In some applications, high-efficiency energy transfer, such as the well-known Förster transfer process which happens when donor−acceptor separation is small, plays a key role in photosynthesis, efficient light-emitting diodes, biological assaying, and lasers.[1] In contrast, in some other important applications, the energy transfer must be reduced or absolutely prevented. For example, in high-order hybrid structures for broadband fiber amplifiers and multicolor volumetric displays,[2] the performance of the system depends strongly on the degree of isolation of discrete dopants. This is because the specific spectrum of one active center must be an integral part of the system.

The existing toolbox for achieving dopant isolation includes approaches of (1) synthesizing active discrete components followed by laminating or incorporating them into a processable matrix[2a,3a] and (2) constraining multiple active centers into a single nanostructure by employing complex core−shell architectures.[3b] Although widely implemented in research, these methods have limitations for practical use because of the need for multistep procedures or the limitation in composite size. In addition, aqueous processing, which is involved in these approaches, cannot eliminate effectively the optical loss induced by hydroxyl or organic species. One possible solution to these problems is to engineer optical properties directly inside the bulk materials. This approach is particularly attractive for three-dimensional (3D) devices. Although various types of glass ceramics (glassy-phase-embedded nanocrytals) have been designed and prepared successfully,[4] there is no report of success in handling interactions among multiple active centers. Here,

† Department of Material Chemistry, Kyoto University.
‡ Arizona State University.
§ Graduate School of Human and Environmental Studies, Kyoto University.
|| Zhejiang University.

(1) (a) Oppenheimer, J. R. *Phys. Rev.* **1941**, *60*, 158. (b) Andrew, P.; Barnes, W. L. *Science* **2000**, *290*, 785–788. (c) Baldo, M. A.; Thompson, M. E.; Forrest, S. R. *Nature* **2000**, *403*, 750–753. (d) Dejneka, M. J.; Streltsov, A.; Pal, S.; Frutos, A. G.; Powell, C. L.; Yost, K.; Yuen, P. K.; Müller, U.; Lahiri, J. *Proc. Natl. Acad. Sci. U.S.A.* **2003**, *100*, 389–393.

(2) (a) Downing, E.; Hesselink, L.; Ralston, J.; Macfarlane, R. *Science* **1996**, *273*, 1185–1189. (b) BallatoJ.; Riman, R. E. U.S. Patent 6,699,406, 2004. (c) Polman, A.; van Veggel, F. C. J. M. *J. Opt. Soc. Am. B* **2004**, *21*, 871–892. (d) Xiao, Z.; Serna, R.; Xu, F.; Afonso, C. N. *Opt. Lett.* **2008**, *33*, 608–610.

(3) (a) Sivakumar, S.; van Veggel, F. C. J. M.; Raudsepp, M. *J. Am. Chem. Soc.* **2005**, *127*, 12464–12465. (b) DiMaio, J. R.; Sabatier, C.; Kokuoz, B.; Ballato, J. *Proc. Natl. Acad. Sci. U.S.A.* **2008**, *105*, 1809–1813.

we introduce an effective approach to control energy transfer between different active centers, based on *in situ* and simultaneous tailoring of the evolution of phases and the distribution of dopants in the glassy phase. We show that the orderly precipitation of multiple types of nanocrystals and the selective incorporation of different dopants into them can be achieved. These help to achieve multicolor visible and broadband near-infrared emission in a single composite having multiple types of doped nanostructures embedded.

Experimental Section

Composites Synthesis. The starting materials for the mother glass were SiO_2, Na_2CO_3, Ga_2O_3, and LaF_3. NiO and ErF_3 were used as source materials for Ni^{2+} and Er^{3+} doping. Since the phase diagram of the investigated system is unavailable, an approximate composition of the glassy phase was chosen by reference to the phase diagram of the system of $SiO_2/Na_2O/Al_2O_3$. To obtain a highly transparent composite, the composition of the glassy phase was further optimized by trial and error. In a typical synthesis, about 20 g of raw materials was mixed completely and melted in a covered corundum crucible at 1450 °C for 30 min in air. The melt was cast into a slab on a stainless steel plate quickly, forming amorphous solids. The as-synthesized samples were treated around glass-transition temperatures to relieve the stress. Subsequently, the samples were heat-treated at the certain temperatures for 2 h in air, inducing precipitation of the designed nanocrystals. Before optical characterizations and space-selective micromachining, the samples were cut into pieces of about $10 \times 10 \times 1.5$ mm^3 and polished carefully.

Physical Measurements of Bulk Samples. Thermal properties of the glass were measured by differential thermal analysis (DTA) at a heating rate of 10 °C/min. The crystalline phases inside the glass were identified by X-ray diffraction (XRD) using Cu Kα radiation (Rigaku RINT-2500HF diffractometer) and a confocal Raman spectrometer (Nanofinder30, Tyoko Instruments Co.) in which a 532 nm excitation laser beam was focused using a 10× objective lens with NA value of 0.25. Since the photoluminescence of Er^{3+} under excitation with the 532 nm laser would induce background noise in the Raman spectrum, the Raman measurement was conducted in an Er^{3+}-free sample. Transmission electron microscopy (TEM) measurements were conducted by using a JEOL 2010F (scanning) transmission electron microscope operating in TEM mode. The absorption spectrum was recorded by using a double-beam spectrometer (JASCO V-570). The visible luminescence of the bulk sample was measured with a fluorescence spectrophotometer (Jobin-Yvon/Horiba Fluoromax-P). The infrared luminescence of the bulk sample was measured with a computer-controlled monochromator under excitation with a 970 nm continuous-wave laser diode. The pumping source was modulated with an LD modulation box by voltage output from a synthesized functional generator, and the signal was detected through a lock-in-amplifier.

Space-Selective Fabrication Using Ultrashort Pulse Laser. A regenerative amplified Ti:sapphire laser (Coherent; Mira and RegA) with a 250 kHz, 80 fs, and 800 nm mode-locked pulse was employed as the external field in the research. Figure S8 in the Supporting Information shows the experimental setup. The laser beam was attenuated to 2.8 μJ by a neutral density filter and then focused inside the glassy sample placed on an *XYZ* stage via a 20× objective lens with NA value of 0.45. Waveguide structure was written inside the glass sample by controlling the sample translation in the *X* direction at a speed of 1 μm/s. For dot structure, 7.5×10^6 successive pulses were sharply focused inside the glass for 30 s, controlled by a mechanical shutter.

Characterization of the Microstructures Induced by Ultrashort Pulse Laser. The sample was polished carefully to expose the microstructures induced by the ultrashort pulse laser before characterizations. To obtain the element distribution map with high contrast, element distributions in the laser-irradiated region were analyzed on the sample with a relatively high doping concentration (1 mol % ErF_3) by using a field-emission electron probe microanalyzer (EPMA) (JXA-8500F). Raman mapping was performed in the confocal Raman spectrometer (Nanofinder30, Tyoko Instruments Co.) in backscattering geometry with a 532 nm laser as excitation source. The laser beam was focused by using a 40× objective lens with NA value of 0.6, which provided scattering areas of ~1 μm^2. The sampling interval was ~1.5 μm. Considering that the luminescence of Er^{3+} causes background noise in the Raman spectrum, the Raman mapping was conducted in an Er^{3+}-free sample. The upconversion luminescence of the laser-induced microstructure was detected by a fiber detector under excitation with the above-mentioned pulse laser. The laser beam was attenuated to 0.08 μJ and then focused by a 50× objective lens with NA value of 0.8. The irradiation area was ~1.2 μm^2, and the sampling interval was ~2 μm.

Results and Discussion

Our strategy in this work is inspired by the metastable nature of the glassy state. In considering the unique local fluctuation characteristic during the crystallization of glassy phase, we envisaged that the resulting local heterogeneity configuration could be designed through presetting an appropriate short-range structure in the mother glassy phase. The target architecture here is a glassy phase which acts a matrix for maintaining three-dimensional networks and supporting crystalline phases, and multiple types of nanocrystals which act not only as domains for dopant isolation but also as the discrete functional components of the composite.

Orderly Precipitation of LaF_3 and Ga_2O_3 Nanocrystals from the Glassy Phase. The first challenge is the *in situ* control of the evolution of multiple types of phases, i.e., the selective precipitation of more than one type of nanocrystals from the glassy phase without obvious reduction of light transparency. The devitrification phenomenon which often occurs during the crystallization process is believed to arise from the collapse of the glassy network, which leads to a dramatic increase of scattering centers such as phase interfaces. To circumvent this problem, we tried to separate the precipitation process, especially the growth stage, of two types of nanocrystals. A prototypical system with -Si-O- as network and -La-F-, -Ga-O- as assemblage units for the desired nucleus was designed, based on the assessment of the thermal diffusivity of ions. In order to obtain the appropriate glassy phase, an exhaustive and systematic study was conducted, using simple and multicomponent glass compositions, by referring to the standard phase diagram of the system of $SiO_2/Na_2O/Al_2O_3$.[5] The optimum composition was $SiO_2/Na_2O/Ga_2O_3/LaF_3 = 51/15/20/14$ in mol %. According to DTA, the glass transition occurred around 580 °C (T_g), followed by two distinct crystallization peaks at 660 (T_{x1}) and 740 °C (T_{x2}), respectively (Supporting Information Figure S1). As

(4) (a) Wang, Y.; Ohwaki, J. *Appl. Phys. Lett.* **1993**, *63*, 3268–3270. (b) Beall, G. H.; Pinckney, L. R. *J. Am. Ceram. Soc.* **1999**, *82*, 5–16. (c) Chiodini, N.; Paleari, A.; Spinolo, G. *Phys. Rev. Lett.* **2003**, *90*, 055507(1)–055507(4). (d) Li, D. L.; Zhou, H. S.; Honma, I. *Nat. Mater.* **2004**, *3*, 65–72. (e) Dantelle, G.; Mortier, M.; Vivien, D.; Patriarche, G. *Chem. Mater.* **2005**, *17*, 2216–2222. (f) Calvez, L.; Ma, H. L.; Lucas, J.; Zhang, X. H. *Adv. Mater.* **2007**, *19*, 129–132. (g) Lahoz, F. *Opt. Lett.* **2008**, *33*, 2982–2984. (h) Chen, D.; Wang, Y.; Yu, Y.; Huang, P. *J. Phys. Chem. C* **2008**, *112*, 18943–18947. (i) Bhattacharyya, S.; Bocker, C.; Heil, T.; Jinschek, J. R.; Höche, T.; Rüssel, C.; Kohl, H. *Nano Lett.* **2009**, *9*, 2493–2496. (j) Tikhomirov, V. K.; Chibotaru, L. F.; Saurel, D.; Gredin, P.; Mortier, M.; Moshchalkov, V. V. *Nano Lett.* **2009**, *9*, 721–724.

(5) Schairer, J. F.; Bowen, N. L. *Am. J. Sci.* **1947**, *245*, 193–204.

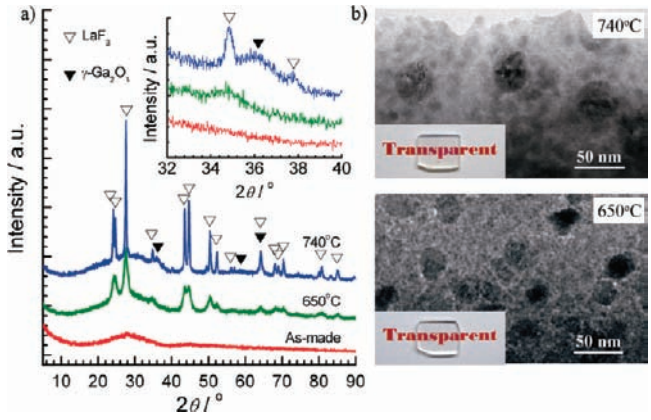

Figure 1. (a) XRD patterns of as-made glass and composites. The inset shows the enlarged part from 32 to 40°. (b) Bright-field TEM images and photographs of the composites treated at 650 and 740 °C, respectively.

shown in Figure 1a, these two crystallization peaks correspond to the precipitation of LaF_3 (JCPDS file no. 32-0483) and Ga_2O_3 (JCPDS file no. 20-0426) nanocrystals, respectively. TEM characterizations of these composites show that heat treatment at 650 °C induced the precipitation of monodispersed nanocrystals an average of 25 nm in diameter, while heat treatment at 740 °C resulted in two types of precipitations: larger nanocrystals (~50 nm in diameter) surrounded by smaller ones (~8 nm in diameter) (Figure 1b). The spherical nanoparticles with larger size are LaF_3, while the smaller nanoparticles are Ga_2O_3. These structural characterizations highlight that the precipitation of two different types of nanocrystals proceeds in a separated manner. Importantly, the obtained composites maintain a high transparency (the inset photographs in Figure 1b) despite the *in situ* precipitation of multiple types of nanocrystals, thus indicating the successful prevention of the collapse of the glass network and demonstrating the feasibility of the proposed strategy.

To gain better knowledge about the subtle structure evolution, we performed a spectroscopic analysis on the composites treated in the temperature range from just above T_g to T_{x2}. Nondoped composite presents an obvious annealing temperature-dependent blue emission (Figure 2a and Supporting Information Figures S2 and S3). The phenomenon can be ascribed to the size-dependent interactions of localized defects in the Ga_2O_3 clusters or/and nanocrystals.[6] It is important to note that the blue luminescence appears just above T_g (580 °C), indicating that the initial nucleation stage of Ga_2O_3 nanocrystals may occur around this temperature, while the recognizable precipitation of Ga_2O_3, corresponding to the growth stage, can only be observed in the sample treated above 700 °C. In contrast, there is no measurable delay between the nucleation and crystal growth stages for the precipitation of LaF_3, which both start just above T_g. Indeed, LaF_3 nanocrystals can be clearly identified in the composite treated at 600 °C (Supporting Information Figure S4). According to the Arrhenius equation, the dynamics of nucleation and growth is dominated by the activation energy (ΔE).[7] We reasoned that the origin of the distinct precipitation dynamics of Ga_2O_3 and LaF_3 was twofold. On one hand, nanometric heterogeneity arising from the density fluctuation in the supercooled solid induces a substantial decrease in the kinetic barrier for nucleation, because the nuclei at the initial precipitation stage can evolve within the denser/cohesive domain. As a result, nucleation of Ga_2O_3 and LaF_3 has very low ΔE, and both can occur at relatively low temperatures (slightly above T_g), leading to a large overlap of their nucleation stage. On the other hand, the remarkable characteristic difference between Ga_2O_3 and LaF_3 may play an important role in the subsequent growth stage. The strong bond strength of Ga−O (>334 kJ/mol)[8] and field strength (F) of Ga^{3+} ($F = 0.75$) substantially slow the crystal growth of Ga_2O_3 due to the necessity of long-range atomic diffusion, resulting in a notable extension of the precipitation temperature span of Ga_2O_3 and a separation of the nanocrystal growth stages of Ga_2O_3 and LaF_3.

Dopant Isolation: Selective Incorporation of Er^{3+} and Ni^{2+} into LaF_3 and Ga_2O_3 Nanocrystals, Respectively. In addition to the purpose of obtaining highly transparent composites, the specific precipitation order of crystalline phases, i.e., LaF_3 followed by Ga_2O_3, may help to solve another, more challenging case, the simultaneous tailoring of the evolution of phases and partitioning of multiple dopants. As a proof-of-concept experiment, erbium (Er^{3+}) and nickel (Ni^{2+}) were selected as dopants, taking into account their fundamental roles in active optical materials.[9] The Er^{3+} single doped system was first examined, and its radiative transitions of $^2H_{11/2} \rightarrow {}^4I_{15/2}$ and $^4S_{3/2} \rightarrow {}^4I_{15/2}$, corresponding to the characteristic emission peaks at 520 and 540 nm, were investigated. With the increase of annealing temperature, the 540 nm emission peak presents a considerable enhancement in intensity, accompanied by an obvious peak splitting, while the 520 nm peak shows only a small change (Figure 2b and Supporting Information Figure S5). This phenomenon can be ascribed to the selective incorporation of some Er^{3+} ions into the crystalline phase, as discussed in Table S1 (Supporting Information). To further clarify the nanocrystal in which some Er^{3+} ions are incorporated, we investigated the LaF_3-free sample, where LaF_3 was replaced by La_2O_3 and only Ga_2O_3 nanocrystals precipitated. It was found that the precipitation of Ga_2O_3, i.e., with the increase of temperature, does not change the fluorescence spectrum of Er^{3+} significantly. On the basis of these two experimental results, it can be supposed that some Er^{3+} ions were selectively incorporated into the LaF_3 nanocrystals. Introduction of the second type of dopant (Ni^{2+}) into Er^{3+}-doped sample makes it appear brown in color and leads to several broad absorption bands with maxima at ~440, ~870, and ~1760 nm (Figure 2c), which can be ascribed to the transitions $^3E'(F) \rightarrow {}^3E''(F)$, $^3E'(F) \rightarrow {}^3A'_2(F)$, and $^3E'(F) \rightarrow {}^3A'_2(P)$ of the trigonal bipyramid fivefold and tetrahedral Ni^{2+} in amorphous matrix.[10] Heat-treatment above 700 °C results in a drastic change in the appearance and absorption characteristic of the sample (Figure 2c). The optical absorption around 600 and 1010 nm represents the typical electronic transitions $^3A_2(F)$

(6) Wang, T.; Farvid, S. S.; Abulikemu, M.; Radovanovic, P. V. *J. Am. Chem. Soc.* **2010**, *132*, 9250–9252.
(7) (a) Ichitsubo, T.; Matsubara, E.; Yamamoto, T.; Chen, H. S.; Nishiyama, N.; Saida, J.; Anazawa, K. *Phys. Rev. Lett.* **2005**, *95*, 245501. (b) Takahashi, Y.; Osada, M.; Masai, H.; Fujiwara, T. *Phys. Rev. B* **2009**, *79*, 214204.
(8) Varshneya, A. K. *Fundamentals of Inorganic Glasses*; Academic Press: San Diego, 1994.
(9) (a) Johnson, L. F.; Dietz, R. E.; Guggenheim, H. J. *Phys. Rev. Lett.* **1963**, *11*, 318–320. (b) Moulton, P. F.; Mooradian, A. *Appl. Phys. Lett.* **1979**, *35*, 838–840. (c) Samson, B. N.; Pinckney, L. R.; Wang, J.; Beall, G. H.; Borrelli, N. F. *Opt. Lett.* **2002**, *27*, 1309–1311. (d) Zhou, S. F.; Dong, H. F.; Feng, G. F.; Wu, B. T.; Zeng, H. P.; Qiu, J. R. *Opt. Express* **2007**, *15*, 5477–5481. (e) Auzel, F. *Chem. Rev.* **2004**, *104*, 139–173. (f) Wang, F.; Han, Y.; Lim, C. S.; Lu, Y.; Wang, J.; Xu, J.; Chen, H.; Zhang, C.; Hong, M.; Liu, X. *Nature* **2010**, *463*, 1061–1065.
(10) Galoisy, L.; Calas, G. *Geochim. Cosmochim. Acta* **1993**, *57*, 3613–3626.

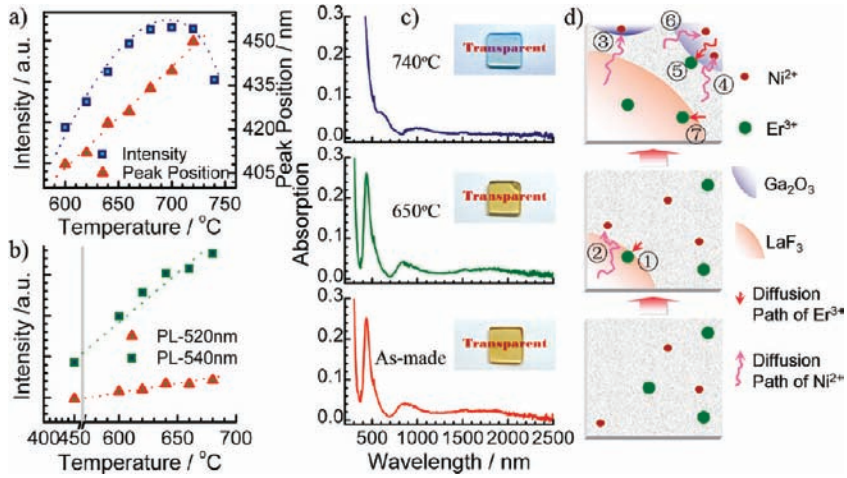

Figure 2. Heat-treatment temperature-dependent blue (a) and green luminescence (b) of Er^{3+}-doped composite. (c) Absorption spectra and corresponding digital photographs of Ni^{2+}-Er^{3+} co-doped as-made sample and composites treated at 650 and 740 °C. (d) Schematic illustrations of the local transitions inside the composite, including nanocrystal growth and dopant diffusion.

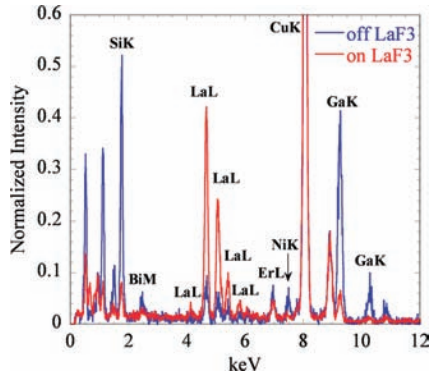

Figure 3. Energy-dispersive X-ray spectroscopy analysis on a single LaF_3 nanoparticle and between two particles. The sample used for analysis is the composite doped with 3 mol % NiO and 3 mol % ErF_3 and treated at 740 °C.

$\rightarrow {}^3T_1(F)$ and ${}^3A_2(F) \rightarrow {}^3T_2(F)$ of octahedral Ni^{2+}.[11] To explore the origin of absorption variation, we performed calculations for the local crystal field strength (D_q) of Ni^{2+} based on the Tanabe−Sugano theory (Supporting Information Table S2).[12] The derived crystal field strength of Ni^{2+} in composite treated at 740 °C is 990 cm^{-1}, larger than that in glass, which is estimated to be about 568 cm^{-1}.[13] A substantial increase (more than 70%) in the crystal field strength of Ni^{2+} during the precipitation of nanocrystals represents the fact that Ni^{2+} incorporates into the crystalline phase, because in general, only a long-range periodic atomic lattice can support high crystal field strength for transition metal ions.[13] Thorough simulations of the theoretical electronic transitions (Table S2) and fits of energy levels of Ni^{2+} (Supporting Information Figure S6) support this statement. Importantly, the increase of crystal field strength follows the growth of Ga_2O_3, rather than that of LaF_3, and spatially resolved energy-dispersive X-ray spectroscopy (EDX) measurements indicate that Ni^{2+} could not be detected on the LaF_3 nanoparticle (Figure 3). These results firmly indicate the selective partition of Ni^{2+} into the Ga_2O_3.

The selective doping phenomenon is primarily associated with the system's tendency to a specific thermodynamic equilibrium and is affected by practical kinetic factors.[14] At the growth stage of LaF_3 nanoparticle, Er^{3+} is expected to incorporate into nanocrystal (path 1, Figure 2d), and Ni^{2+} probably diffuses out from the crystalline phase-rich region (path 2, Figure 2d), because of the striking similarity between La^{3+} and Er^{3+}, including large size ($r_{La^{3+}} = 1.300$ Å; $r_{Er^{3+}} = 1.144$ Å),[15] high valence state and field strength ($F_{La^{3+}} = 0.482$; $F_{Er^{3+}} = 0.539$), and large difference between La^{3+} and Ni^{2+} ($r_{Ni^{2+}} = 0.83$ Å).[15] Accordingly, selective trapping of Ni^{2+} (paths 3, 4, and 6, Figure 2d) rather than Er^{3+} (path 5, Figure 2d) in the Ga_2O_3 precipitation region is favorable for Gibbs free energy minimization, considering the appropriate environment provided by that Ga_2O_6 octahedron ($r_{Ga^{3+}} = 0.76$ Å; $F_{Ga^{3+}} = 0.75$) for Ni^{2+}.[15] In addition to the influence of ionic radius and field strength, we supposed that the electron configuration of dopants also contributed much to the selective doping phenomenon. To confirm this point, we calculated the crystal field stabilization energy (CFSE) of Ni^{2+} and Er^{3+} in different coordination sites. Since each electron in a t_{2g} orbital stabilizes a transition metal ion in octahedral coordination by $4D_q$, and each electron in an e_g orbital stabilizes it by $6D_q$, CFSE of octahedral Ni^{2+} in Ga_2O_3 can be estimated to be −142 kJ/mol, and that of tetrahedral Ni^{2+} in Ga_2O_3 and glassy phase is about −40 kJ/mol.[13] In comparison, Er^{3+} has relative low CFSE, around −0.78 kJ/mol in the octahedral position and −0.73 kJ/mol in a cubic environment.[16] The high octahedral site preference energy (−102 kJ/mol) of Ni^{2+}, which originates from its unique $(t_{2g})^6(e_g)^2$ electron configuration with two unpaired electrons, can be expected to drive Ni^{2+} to selectively substitute for octahedral Ga, since it is the only available octahedral position in the composite, thus resulting in an enrichment of Ni^{2+} in the Ga_2O_3 nanocrystal.

To explore the isolation degree between Er^{3+} and Ni^{2+} ions in the obtained composite, we made a close inspection of the absorption spectra of Ni^{2+} and local element distribution analysis. It is significant to find that the characteristic absorption peaks of Ni^{2+} in glass have completely disappeared once the

(11) Moncorgé, R.; Benyattou, T. *Phys. Rev. B* **1988**, *37*, 9186–9196.
(12) Tanabe, Y.; Sugano, S. *J. Phys. Soc. Jpn.* **1954**, *9*, 766–779.
(13) Burns, R. G. *Mineralogical Applications of Crystal Field Theory*; Cambridge Univ. Press: Cambridge, 1993.
(14) (a) Erwin, S. C.; Zu, L.; Haftel, M. I.; Efros, A. L.; Kennedy, T. A.; Norris, D. J. *Nature* **2005**, *436*, 91–94. (b) Norris, D. J.; Efros, A. L.; Erwin, S. C. *Science* **2008**, *319*, 1776–1779. (c) Wang, F.; Liu, X. G. *J. Am. Chem. Soc.* **2008**, *130*, 5642–5643.
(15) Shannon, R. D. *Acta Crystallogr. A.* **1976**, *32*, 751–767.
(16) Yatsimirskii, K. B.; Kostromina, N. A. *Theor. Exp. Chem.* **1966**, *2*, 436–439.

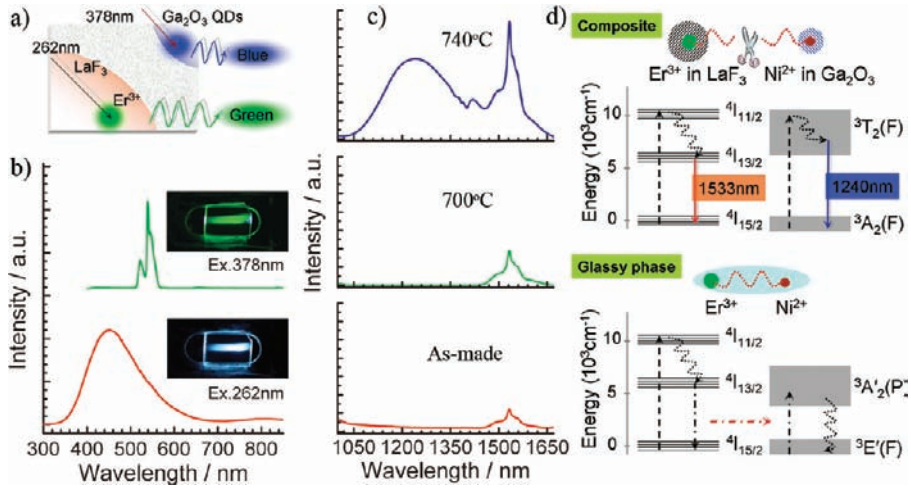

Figure 4. (a) Sketch of the origin of switchable two-color emission. (b) Visible luminescence spectra and photographs of the transparent Er^{3+}-doped composite treated at 720 °C under excitation with 262 and 378 nm. (c) Near-infrared luminescence spectra of $Er^{3+}-Ni^{2+}$ co-doped as-made sample and composites treated at 700 and 740 °C under excitation with a 980 nm laser diode. (d) Proposed mechanisms of energy transfer and radiative/irradiative electron transitions in $Er^{3+}-Ni^{2+}$ co-doped glassy phase and composite. The dashed, dotted, dashed-dotted, and full arrows represent photon excitation, irradiative multiphonon relaxation, energy transfer, and emission process, respectively.

Ga_2O_3 nanocrystals precipitate (Figure 2c and Supporting Information Figure S7), indicating the high efficiency of doping Ni^{2+} into Ga_2O_3. This is consistent with the EDX results (Figure 3). On the basis of these investigations, it can be concluded that the isolation degree between Er^{3+} and Ni^{2+} is high, although a lot of Er^{3+} ions are also detected in the glassy phase (Figure 3). The difference in doping efficiency between Er^{3+} and Ni^{2+} can be ascribed to the disparity in their diffusion ability and CFSE. In consideration of the *in situ* activation characteristic of dopants in the glassy phase and the high diffusion ability of Ni^{2+} compared with Er^{3+}, the designed precipitation habit is helpful for achieving a high isolation degree: large LaF_3 and small Ga_2O_3 particles result in more efficient trapping of Er^{3+} within LaF_3 (path 7, Figure 2d) and exclusion of Er^{3+} from the Ga_2O_3 precipitation region (path 5, Figure 2d) without much influence on the selective doping of Ni^{2+} into Ga_2O_3 (paths 2, 3, 4, and 6, Figure 2d).

Multicolor Visible and Broadband Near-Infrared Luminescence from the Composite. The success in selectively squeezing two types of homogeneously distributed emission centers into different, highly confined geometries by local structure arrangement provides a great convenience for construction of new multifunctional composites through design of the discrete functional components. For example, introduction of Er^{3+} into the transparent composite treated at 720 °C induces bright, switchable two-color luminescence, blue to green, simply by tuning the excitation wavelength from 262 to 378 nm, which benefits from the suppression of energy transfer between Ga_2O_3 quantum dots and Er^{3+} (Figure 4a,b). Energy-transfer control in the obtained composite offers another opportunity in the development of a broadband light source. We prepared and investigated the $Er^{3+}-Ni^{2+}$ co-doped composite with well-defined doping concentrations (0.05 mol % Er^{3+} and 0.1 mol % Ni^{2+}). It is interesting to find that the composite treated at 740 °C presents a unique ultra-broadband near-infrared emission under excitation with a single 980 nm laser diode, which covers the whole telecommunication low-loss window (1200−1600 nm) (Figure 4c). The observed two emission bands with the central wavelength at 1240 and 1533 nm originate from the $^3T_2(F) \rightarrow {}^3A_2(F)$ transition of Ni^{2+} and the $^4I_{13/2} \rightarrow {}^4I_{15/2}$ transition of Er^{3+}, respectively. In contrast, the composites treated at low temperatures without the efficient separation of two centers show only very weak and narrow emission around 1533 nm because of the prevailing energy transfer between Ni^{2+} and Er^{3+} (Figure 4c,d).

It is significant to discuss further how the selective partition of dopants modifies their independent or collaborative electron transitions. Once Ni^{2+} and Er^{3+} ions process a selective doping, the average separation distance between them is expected to increase because of the self-cataloging effect. This results in a decrease of energy-transfer rate, K_T, according to the energy-transfer relation $K_T \alpha r^{-6}$, where r is the separation distance.[17] Another factor contributing to the limited energy transfer in our system is the variation of the local crystal field around active centers during the formation of nanocrystals. For a specific donor−acceptor coupler, the inherent tendency to energy-transfer is defined by the critical distance R_0, which can be calculated from the expression $R_0 = (2.11 \times 10^{-2})[\kappa^2 \eta^{-4} Q_D \int \varepsilon_A(\lambda) F_D(\lambda) \lambda^4 \, d\lambda]^{1/6}$, where κ^2 is the dipole orientation factor, η is the refractive index of the medium, Q_D is the quantum yield of the donor, and $\int \varepsilon_A(\lambda) F_D(\lambda) \lambda^4 \, d\lambda$ represents the spectra overlap integral of donor emission and acceptor absorption. It is interesting to note that the lowest excited state of Ni^{2+} shifts to a high-energy position under the environment of high crystal field strength provided by Ga_2O_3, whereas the energy levels of Er^{3+} show negligible changes after incorporation into the LaF_3 nanocrystal (Figure 4d). This difference induces a decrease in the spectral overlap between the lowest excited states of Ni^{2+} and Er^{3+} which dominate the energy transfer, thus resulting in a reduction in critical distance and energy-transfer probability. Hence, both separation distance and spectral overlap contribute significantly to the energy-transfer control in our system, and in marked contrast to the method using core−shell structure, where only one variable of separation distance can be tuned,[3b] the strategy here is expected to enable improvements in our ability to manage energy transfer because of the special synergistic effect.

(17) Förster, T. *Discuss. Farad. Soc.* **1959**, *27*, 7–17.

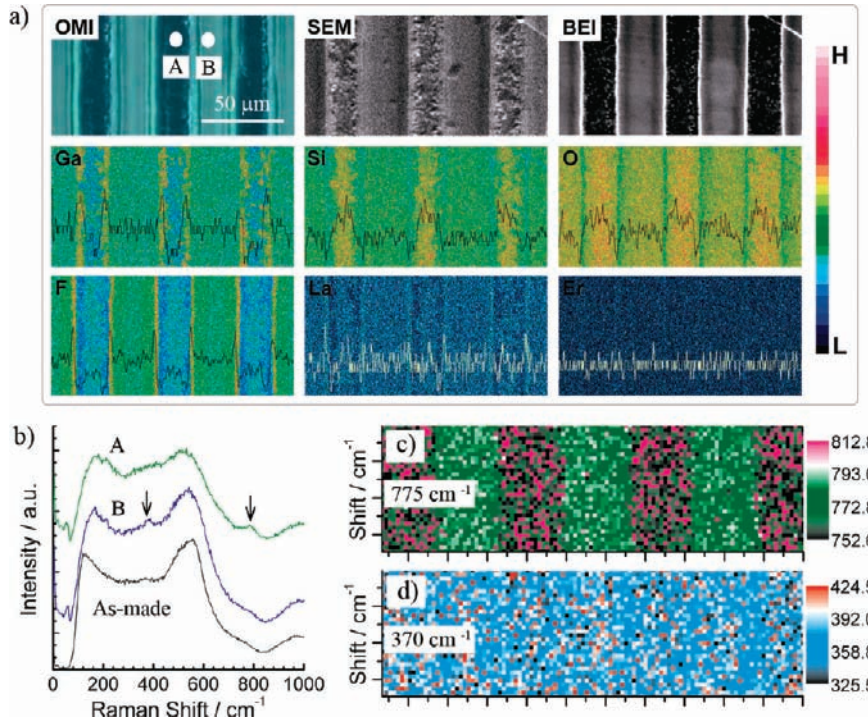

Figure 5. (a) Optical microscope image (OMI), scanning electron microscopy (SEM), backscattering electron image (BEI), and EPMA mapping showing the ultrashort laser pulse-induced microstructure and relative concentration change of different ions. (b) Micro-Raman spectra of as-made sample and the laser-modified zone (A,B) shown in the microscope image. (c,d) Micro-Raman mapping at 775 and 370 cm^{-1}, which are the characteristic peaks of crystalline Ga_2O_3 and LaF_3, respectively.

Space-Selective Simultaneous Tailoring of Phase Evolution and Dopant Distribution. We further expected that the space-selective simultaneous tailoring of the phase evolution and dopant distribution can be realized by controlling the distribution of the stimulation field. With the benefit of ultrashort pulse duration, the femtosecond pulse laser has been proved to be a powerful tool for space-selective fabrication of the desired microstructure with high precision.[18] To achieve the target, an ultrashort pulse laser (80 fs) was employed, and the repetition rate was tuned to be 250 kHz to obtain the necessary heat accumulation (Supporting Information Figure S8). As a model system for realization of the goal, parallel waveguide structure was drawn inside the as-made sample. As shown in Figure 5a, no obvious crack can be observed. The contrast in the optical microscope image can be ascribed to the index change after femtosecond pulse laser irradiation. The induced structure was characterized by using an EPMA (Figure 5a). Notably, a microheterogeneous spatial distribution of elements can be observed in the patterned area. Si/O and La/Er/F are enriched in the middle and the edge region, respectively; most Ga is sandwiched between them, and some of it can also be detected in the central part of the structure. This local element redistribution is related to the nonequilibrium−equilibrium states transition under focused laser irradiation, and the specific element distribution order could be partly explained by the difference in ionic diffusion coefficients. The relatively high bond strength of Ga−O compared with that of La(Er)−F corresponds to the large diffusion activation energy of Ga, leading to the preferential occupation of Ga close to the focal point. This collaborates with the initially proposed strategy. Figure 5b shows the Raman scattering spectra of the sample before and after laser irradiation. Two new sharp peaks at ~370 and 775 cm^{-1} observed in the Raman spectra of different area can be ascribed to the characteristic peaks of crystalline LaF_3 and Ga_2O_3, respectively.[19] To further investigate the crystalline phase distribution, Raman scattering mapping analysis was performed. The Raman mapping picture of Ga_2O_3 (775 cm^{-1}) clearly shows the profile of the defined waveguide structure (Figure 5c). The Raman mapping picture of LaF_3 (370 cm^{-1}) exhibits a low contrast which is primarily due to the strong background around this wavelength; however, the alternatively distributed pattern can still be distinguished (Figure 5d). The results reveal that the crystalline Ga_2O_3 and LaF_3 dominate the center and the edges of the induced structure, respectively, thus demonstrating the success in the simultaneous spatial control of phase evolution and element distribution.

The key advantage of three-dimensional simultaneous tailoring of the phase evolution and dopant distribution in a composite is that it allows us to space-selectively engineer its optical properties. We investigated the up-conversion luminescence of Er^{3+} and Ga_2O_3 quantum dots along the direction marked by the white arrow in Figure 6a. Since the 520 nm peak of Er^{3+} shows only a small change during the process of crystallization, we use the intensity ratio between two peaks of Er^{3+} (PL_{540}/PL_{520}) to represent the enhancement of green luminescence

(18) (a) Shimotsuma, Y.; Kazansky, P. G.; Qiu, J. R.; Hirao, K. *Phys. Rev. Lett.* **2003**, *91*, 247405(1)–247405(4). (b) Juodkazis, S.; Nishimura, K.; Misawa, H.; Ebisui, T.; Waki, R.; Matsuo, S.; Okada, T. *Adv. Mater.* **2006**, *18*, 1361–1364. (c) Kanehira, S.; Miura, K.; Hirao, K. *Appl. Phys. Lett.* **2008**, *93*, 023112(1)–023112(3). (d) Yang, W.; Corbari, C.; Kazansky, P. G.; Sakaguchi, K.; Carvalho, I. C. S. *Opt. Express* **2008**, *16*, 16215–16226. (e) Gattass, R. R.; Mazur, E. *Nat. Photonics* **2008**, *2*, 219–225.

(19) (a) Liarokapis, E.; Anastassakis, E.; Kourouklis, G. A. *Phys. Rev. B* **1985**, *32*, 8346–8355. (b) Choi, Y. C.; Kim, W. S.; Park, Y. S.; Lee, S. M.; Bae, D. J.; Lee, Y. H.; Park, G.; Choi, W. B.; Lee, N. S.; Kim, J. M. *Adv. Mater.* **2000**, *12*, 746–750.

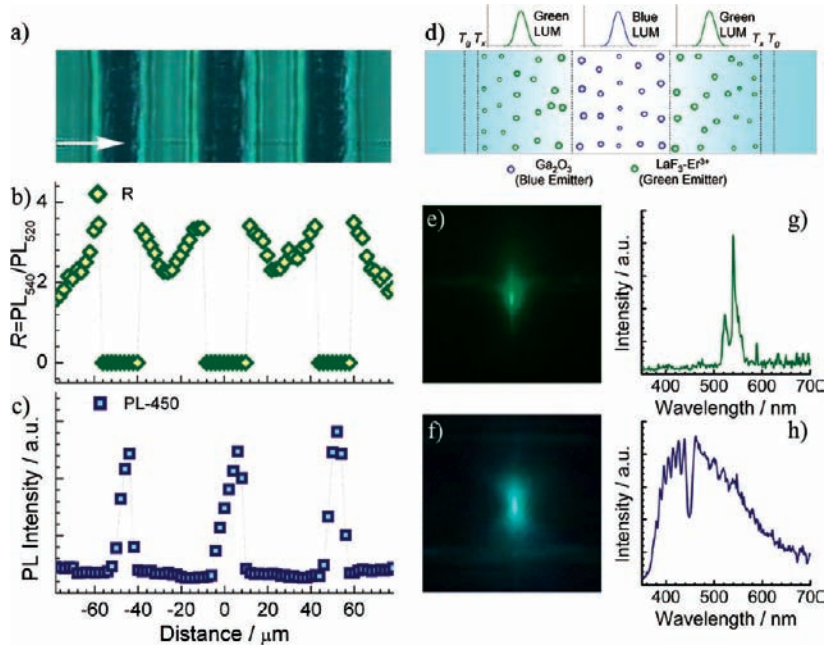

Figure 6. (a) Optical microscope image of the induced structure. Photoluminescence was studied along the direction marked by the white arrow. (b,e,g) and (c,f,h) Emission distribution, typical true-color optical microscope images, and corresponding spectra of green and blue emission, respectively. (d) Schematic illustration the origin of the alternative green−blue emission distribution.

resulting from the microstructure change around the active center. The induced structure shows a remarkable alternative green and blue luminescence, as shown in Figure 6b−h. The zero ratio in Figure 6b represents no obvious green luminescence. Importantly, the spatially defined emission presents a sharp contrast, with pure blue (Figure 6f,h) and green (Figure 6e,g) color in the center and at the edge of the induced structure, respectively, which results mainly from the well-controlled distribution of phases and active centers. The intense green luminescence at the edge can be ascribed to the high Er^{3+} concentration and selective doping of Er^{3+} into LaF_3 nanocrystals in this region, which is demonstrated by EPMA and Raman scattering characterization in Figure 5. In comparison, the distribution of blue emission, with the highest intensity in the center of the structure, is abnormally contrary to that of Ga content, with the lowest concentration in this region (Figure 5a). The phenomenon is very similar to the heat-treatment temperature-dependent luminescence observed in Figure 2a. This is primarily ascribed to the crystal-size-determined optical properties of Ga_2O_3 nanocrystals, which results in the optimal luminescence occurring in the moderate-size Ga_2O_3 nanocrystals. During laser scanning, the successive heat-treatment effect on the irradiated region can induce a quite different growth rate of Ga_2O_3 nanocrystals in different regions, with the high growth rate and large-size nanocrystals in the Ga-rich region and the relatively low growth rate and small-size nanocrystals in the Ga-poor region. Additionally, the stabilization effect of the viscous Si−O network can also lead to a remarkable suppression of nanocrystal growth in the central region, where SiO_2 exhibits a relatively high concentration (Figure 5a). A simplified model for explaining the rearrangement of active centers after laser irradiation is shown in Figure 6d.

That the employed ultrashort pulse laser is adjustable enables us to control the "stimulating field" in a rational way. In a separate experiment, we set a dot-by-dot drawing configuration for the purpose of avoiding the successive heat-treatment effect during stimulation (Supporting Information Figure S9). Unlike the continuous scan mode, the dot-by-dot irradiation mode can provide an exceptionally high quenching rate in the local region. As shown in Figure S9, this mode helps us to obtain a ring-shape distributed and improved blue luminescence which benefits from the substantial suppression of Ga_2O_3 nanocrystal growth. We supposed that the fine control of related parameters such as pulse width, repetition rate, and beam shape would help us to create a diversity of active microstructures.

Conclusions

In conclusion, we have demonstrated a novel and effective strategy to achieve energy-transfer control between different active centers by *in situ* simultaneous tailoring of the phase evolution and dopant distribution in the glassy phase. By control of the precipitation habit of multiple crystalline phases (Ga_2O_3 and LaF_3), active centers (Er^{3+} and Ni^{2+}) can be efficiently isolated by selective partitioning into different crystalline phases. Benefitting from the dual effects of physical separation and local crystal field change, the energy transfer between different active centers can be remarkably suppressed, leading to a unique multicolor visible and ultra-broadband near-infrared luminescence of the obtained composite. This strategy can potentially solve several sticky problems in the fabrication of functional light sources by the conventional method. For example, multicolor emission achieved in a single composite can overcome the device integration difficulty encountered in the traditional approach, which is mainly based on mechanical combination of mature, single-color-emitting components.[2a,20] The high transparency of the composite is an especially great advantage for highly efficient excitation and compact 3D display application. In addition, the ultra-broadband light source using a single pump scheme which covers the whole telecommunication low-loss window (1200−1600 nm) has fundamental applications as a compact multiband fiber amplifier, and in stark contrast to

(20) Ananias, D.; Ferreira, A.; Carlos, L. D.; Rocha, J. *Adv. Mater.* **2003**, *15*, 980–985.

other methods such as aqueous processing, the synthetic approach here is based on mature dry-fiber fabrication technology, providing more interfaces for large-scale production. We anticipate that the strategy can be expanded to a broad range of important host/activator combinations. Moreover, the strategy is successfully extended to accomplish three-dimensional simultaneous tailoring of the phase evolution and dopant distribution by employing a modulated stimulation field (ultrashort pulse laser), thus further promising an improved ability for space-selective fabrication of various types of active microstructures and construction of three-dimensional active photonics components with high compactness.

Acknowledgment. This work was supported by the Japan Society for the Promotion of Science (JSPS) (Grant No. 21·09056). This work was also supported by the National Natural Science Foundation of China (Grant Nos. 50872123 and 50802083). S.Z. is grateful for the support from JSPS in the form of a fellowship. The authors are grateful to A. Stone, S. Kanehira, J. Ueda, S. Ye, Y. Hamada, X. Wang, N. Wu, and Y. Teng for their kind suggestions and help on some experiments.

Supporting Information Available: DTA of the as-made glassy phase, PLE and PL spectra of the nondoped composite treated at 700 °C, annealing temperature-dependent peak position of PLE spectra of blue luminescence, XRD pattern of the composite treated at 600 °C for 2 h, luminescence spectra of Er^{3+}-doped as-made glass and the composite treated at 680 °C for 2 h, reduced matrix elements of Er^{3+}, crystal field simulation on Ni^{2+}, energy levels of Ni^{2+} in the composite treated at 710 °C, absorption spectra of $Ni^{2+}-Er^{3+}$ co-doped glass and the composite heat-treated at 650 and 710 °C, schematic illustration of the experimental setup for space-selective microfabrication and upconversion luminescence measurement, and EPMA and PL investigation of the laser-modified region fabricated by dot-by-dot mode. This material is available free of charge via the Internet at http://pubs.acs.org.

JA108512G